Harmonic oscillations of a circular cylinder moving with constant velocity in a quiescent fluid

Jan Novaes Recicar
Instituto de Engenharia Mecânica – Unifei.
Itajubá – MG [Brasil]
recicar@unifei.edu.br

Luiz Antonio Alcântara Pereira
Instituto de Engenharia Mecânica – Unifei.
Itajubá – MG [Brasil]
luizantp@unifei.edu.br

Miguel Hiroo Hirata
FAT/UERJ – Campus Regional de Resende.
Resende – RJ [Brasil]
hirata@fat.uerj.br

The flow around an oscillating circular cylinder which moves with constant velocity in a quiescent Newtonian fluid with constant properties is analyzed. The influences of the frequency and amplitude oscillation on the aerodynamic loads and on the Strouhal number are presented. For the numerical simulation, a cloud of discrete Lamb vortices are utilized. For each time step of the simulation, a number of discrete vortices are placed close to the body surface; the intensity of theirs is determined such as to satisfy the no-slip boundary condition.

Key words: Aerodynamic loads. Oscillating body. Panels methods. Strouhal number. Vortex method.

1   Introduction

Understanding and being able to analyze the flow around an oscillating body which moves with constant velocity in a quiescent fluid with constant properties is of great fundamental and practical importance in aero and hydrodynamics analysis. Oscillatory motions of small amplitude are important in the analysis of immerse vibrating bodies and special care should be taken in the lock-in condition. Large amplitude motions, on the other hand, are of relevance in the analysis of bodies located in waves and currents such as the ones found in the offshore structures (WILLIAMSON; ROSHKO, 1988).

The oscillatory motion of small amplitude mainly modifies the near field changing the boundary layer flow and, as a consequence, having an important effect on the aerodynamic forces and the pressure distribution. If the amplitude of the oscillatory motion is large one observes, additionally, substantial changes in the far field wake which can be of importance in the presence of other bodies or near by surfaces.

This paper deals with the analysis of a body oscillating around a fixed position which is located in an incoming uniform flow with constant velocity; to simplify matters the oscillatory motion is restricted to heave. In previous works, Silva (2004) analyzed the same situation with the restriction of small amplitude of oscillation and Mustto et al. (1998) presented results for a rotating cylinder.

A simpler approach to the present problem would consider a fixed body located in an oscillating incoming flow; notice, however, that with this approach the whole fluid mass would oscillate with the same frequency and amplitude, which is not quite what, happens in real situations, mainly in the far field region.

For the numerical simulations a Lagrangian approach is used, more specifically the Vortex Method (CHORIN, 1973), (LEWIS, 1999), (KAMEMOTO, 1994, 2004), (SARPKAYA, 1994), (HIRATA et al., 2003). In the Lagrangian discrete vortex method, the vorticity generated on the body surface is discretized and represented by a cloud of particles carrying vorticity. Lamb vortices with a viscous core are used for that matter (MUSTTO et al., 1998).

Results for a circular cylinder fixed and heaving in a uniform flow are presented and compared with results found in the literature; these are experimental results as well as results obtained using numerical simulations. It is important to mention that although the Reynolds number used in the simulations is high, no attempt to include turbulence modeling (ALCÂNTARA PEREIRA et al., 2002) was made.

In the present simulations the integrated aerodynamic loads (such as lift and drag coefficient), the pressure distribution and the Strouhal number agree quite well with the experimental results when the cylinder is kept without oscillation. Due to the alternate vortex shedding the lift coefficient oscillates, around zero, during the numerical simulation; the amplitude of the lift coefficient oscillation is increased with the cylinder oscillation keeping, however, the mean value almost identically to zero.

It is also possible to identify three different types of flow regime as the cylinder oscillation frequency increases. The first type – Type I – is observed for low frequency range of the cylinder oscillation; in this situation the Strouhal number remains almost constant. Type I is followed by an intermediate range of frequency – Type II, the transition regime – where apparently the shedding frequency does not correlate to the frequency of the cylinder oscillation. Finally, in Type III – high frequency of cylinder oscillation – the vortex shedding frequency is locked-in with the cylinder oscillation frequency.

2 Problem definition and mathematical model

2.1 Definitions

Consider the incompressible flow (of a Newtonian fluid) around a moving body in a large two-dimensional domain. The body moves to the left with constant velocity; an oscillatory motion with finite amplitude A and constant angular velocity ω is added to body motion.

This is represented, in Fig. 1, by a heaving cylinder immersed in a uniform incoming flow with velocity U. In this figure the (x, o, y) is the inertial frame of reference and the (X, O, Y) is the coordinate system fixed to the cylinder; this coordinate system oscillates around the x-axis as $y_o = A\cos(\omega t)$.
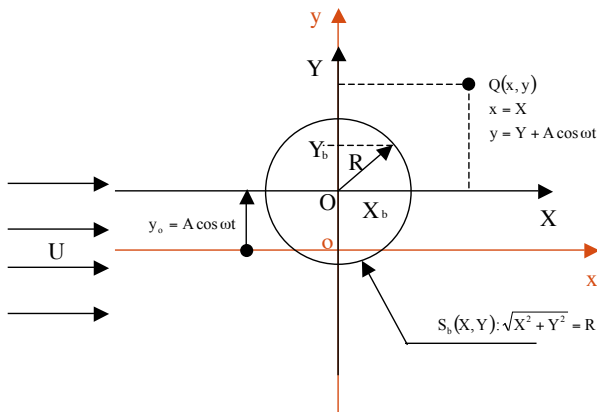
Figure 1: Problem definition
Source: the authors.

The boundary S of the fluid domain is $S = Sb \cup S_\infty$; being S_∞ the far away boundary, which can be viewed as $r = \sqrt{x^2 + y^2} \rightarrow \infty$, and S_b the body surface.

In the body fixed coordinate system, the surface S_b is defined by the function

$$F_b(X,Y) = Y_b - \eta(X) = 0$$

(1)

Thus, in the inertial frame of reference

$$S_b : F_b(x,y,t) = y_b - [y_0(t) + \eta(x)] = 0$$

(2)

and, for a symmetrical body

$$F_b(x,y,t) = y_b - y_0(t) \pm \eta(x) = 0$$

(3).

2.2 Governing equations

For an incompressible fluid flow the continuity is written as

$$\nabla \cdot u = 0$$

(4)

where $\mathbf{u} \equiv (u, v)$ is the velocity vector.

If, in addition, the fluid is Newtonian with constant properties the momentum equation is represented by the Navier-Stokes equation as

$$\frac{\partial u}{\partial t} + u \cdot \nabla u = -\nabla p + \frac{1}{Re}\nabla^2 u$$

(5)

Re stands for the Reynolds number defined as $Re = \dfrac{bU}{\upsilon}$ where b = d = cylinder diameter.

On the body surface the adherence condition has to be satisfied. This condition is better specified in terms of the normal and tangential components as

$$(u \cdot n) = (v \cdot n)$$

(6)

on S_b, the impenetrability condition

$$(u \cdot \tau) = (v \cdot \tau)$$

(7)

on S_b, the no-slip condition

here $\mathbf{n}$ and τ are unit normal and tangential vectors, $\mathbf{u}$ is the fluid particle velocity and $\mathbf{v}$ is the body surface velocity.

Far from the body one assumes that the perturbation due to the oscillating body fades away, that is

$$|u| \rightarrow 1 \tag{8}$$

One should mention that the above boundary value problem was made non-dimensional using **U** and **d** as characteristic quantities.

3 The vortex method

3.1 Viscous splitting algorithm and aerodynamics loads

Taking the curl of the Navier-Stokes equation and with some algebraic manipulations, one gets the vorticity equation which presents no pressure term. In two-dimensions, this equation reads

$$\frac{\partial \omega}{\partial t} + u \cdot \nabla \omega = \frac{1}{Re} \nabla^2 \omega \tag{9}$$

which is an scalar equation since ω is the only component of the vorticity vector $\omega = \nabla \times u$.

The left hand side of the above equation carries all the information needed for the convection of vorticity while the right hand side governs the diffusion. Following Chorin (1973), we use the viscous splitting algorithm, which, for the same time step of the numerical simulation, says that

Convection of vorticity is governed by

$$\frac{\partial \omega}{\partial t} + u \cdot \nabla \omega = 0 \tag{10}$$

Diffusion of vorticity is governed by

$$\frac{\partial \omega}{\partial t} = \frac{1}{Re} \nabla^2 \omega \tag{11}$$

Having determined the vorticity field the pressure calculation starts with the Bernoulli function, defined by Uhlman (1992) as

$$Y = p + \frac{u^2}{2}, \quad u = |u| \tag{12}$$

Following Shintani and Akamatsu (1994), this function is then obtained using the following integral formulation

$$H\overline{Y_i} - \int_{S_1} \overline{Y} \nabla G_i \cdot e_n dS = \iint_{\Omega} \nabla G_i \cdot (u \times \omega) d\Omega - \frac{1}{Re} \int_{S_1} (\nabla G_i \times \omega) \cdot e_n dS \tag{13}$$

where H = 1 in the fluid domain, H = 0.5 on the boundaries and G is a fundamental solution of the Laplace equation, Alcântara Pereira et al. (2002).

3.2 Convection and diffusion of vorticity

For the numerical implementation, the vorticity in the fluid domain is simulated by a cloud of Lamb vortices.

For each time step of the simulation, a number of discrete vortices are generated on the body surface; the intensity of these newly generated vortices is determined using the no-slip condition, see Eq. (7).

For the convection of the discrete vortices of the cloud, Eq. (10) is written in its Lagrangian form as

$$\frac{dx^{(i)}}{dt} = u^{(i)}(x, y, t) \tag{14a}$$

$$\frac{dy^{(i)}}{dt} = v^{(i)}(x, y, t) \tag{14b}$$

being i = 1, N; N is the number of vortices in the cloud.

A second order solution to this equation is given by the Adams-Bashforth formula (FERZIGER, 1981)

$$x^{(i)}(t + \Delta t) = x^{(i)}(t) + \left[1.5u^{(i)}(t) - 0.5u^{(i)}(t - \Delta t)\right]\Delta t$$

(15a)

$$y^{(i)}(t + \Delta t) = y^{(i)}(t) + \left[1.5v^{(i)}(t) - 0.5v^{(i)}(t - \Delta t)\right]\Delta t$$

(15b)

The diffusion of vorticity is taken care of using the random walk method (LEWIS, 1991). The random displacement $Z_d \equiv (x_d, y_d)$ is defined as

$$x_d^{(i)} = \left[\cos(2\pi Q)\right]\sqrt{\frac{4\Delta t}{Re}\ln\left(\frac{1}{P}\right)}$$

(16a)

$$y_d^{(i)} = \left[\sin(2\pi Q)\right]\sqrt{\frac{4\Delta t}{Re}\ln\left(\frac{1}{P}\right)}$$

(16b)

Therefore the final displacement is written as

$$x^{(i)}(t + \Delta t) = x^{(i)}(t) + \left[1.5u^{(i)}(t) - 0.5u^{(i)}(t - \Delta t)\right]\Delta t + x_d^{(i)}$$

(17a)

$$y^{(i)}(t + \Delta t) = y^{(i)}(t) + \left[1.5u^{(i)}(t) - 0.5v^{(i)}(t - \Delta t)\right]\Delta t + y_d^{(i)}$$

(17b)

4   Numerical implementation

The $u^{(i)}$ and $v^{(i)}$ components of the velocity induced at the location of the (i) vortex can be written as

$$u^{(i)} = ui^{(i)} + uc^{(i)} + uv^{(i)}$$

(18a)

$$v^{(i)} = vi^{(i)} + vc^{(i)} + vv^{(i)}$$

(18b)

where:

$\mathbf{ui}^{(i)} \equiv [ui^{(i)}, vi^{(i)}]$ is the incident flow velocity,

$\mathbf{uc}^{(i)} \equiv [uc^{(i)}, vc^{(i)}]$ is the velocity induced by the cylinder at the location of vortex (i),

$\mathbf{uv}^{(i)} \equiv [uv^{(i)}, vv^{(i)}]$ is the velocity induced at the vortex (i) by the other vortices of the cloud.

The $\mathbf{ui}^{(i)}$ and $\mathbf{uv}^{(i)}$ calculations present no problems and they follow the usual Vortex Method procedures; to the first approximation the same happens with the $\mathbf{uc}^{(i)}$ when the body oscillation amplitude is small, see Silva (2004).

For large amplitude body oscillations, however, the body boundary conditions can not be transferred from the actual position to the mean position. As the body surface is simulated by NP straight line panels on which singularities are distributed (Panels Method) it is convenient to calculate the body induced velocity in the moving coordinate system. For that one has to observe the following

– The fluid velocity on the body surface is written as

$$u(X, Y; t) = Ui - \dot{y}_0(t); \text{ with } \dot{y}_0(t) = \frac{d}{dt}\left[A\cos(\omega t)\right]$$

(19)

As a consequence of the j component of the right hand side of the fluid velocity (in the above expression) one gets an additional singularities distribution on the body surface. Of course, the induced velocity due to this additional singularities distribution fades away from the body.

– The velocity induced by the body, according to the panel method calculations, is indicated by [uc(X,Y), vc(X,Y)]; this is the velocity induced at the vortex (i), located at the point [x(t), y(t)]; thus

$$uc^{(i)}(x,y;t) = uc(X,Y;t) \tag{20a}$$

$$vc^{(i)}(x,y;t) = vc(X,Y;t) + \dot{y}_0(t) \tag{20b}$$

where the following relations remains

$$x^{(i)}(t) = X \tag{21a}$$

$$y^{(i)}(t) = y_0(t) + Y \tag{21b}$$

The drag and lift coefficients can be expressed by (Ricci, 2002)

$$C_D = -\sum_{j=1}^{NP} 2(p_j - p_\infty)\Delta S_j \sin\theta_j = -\sum_{j=1}^{NP} C_P \Delta S_j \sin\theta_j \tag{22a}$$

$$C_L = -\sum_{j=1}^{NP} 2(p_j - p_\infty)\Delta S_j \cos\theta_j = -\sum_{j=1}^{NP} C_P \Delta S_j \cos\theta_j \tag{22b}$$

where ΔS_j is the panel length and θ_j represents the panel angle.

5 Results

We start presenting the results for a stand still circular cylinder immersed in a uniform flow. Table 1 shows the results for a circular cylinder, Re = 10^5. Line 1 (BLEVINS, 1984) are experimental results while line 2 (MUSTTO et al., 1998) and line 3 (ALCÂNTARA PEREIRA et al., 2002) are numerical results obtained using different implementation of the Vortex Method. The results presented

in line 4, as well as all the other results presented elsewhere in this paper were obtained carrying out the simulations with M=50 sources panels to replace the cylinder surface and lasted for t = 40 dimensionless time. In each time step, the nascent vortices were placed into the cloud through a displacement $\varepsilon = \sigma_0 = 0.0009b$ normal to the panels. As mention before, no attempt to include turbulence modeling (ALCÂNTARA PEREIRA et al., 2002) in the algorithm was made.

Table 1: Lift and drag coefficients and Strouhal number for a circular cylinder

Re = 10^5, A = 0 and ω = 0	$\overline{C}_L$	$\overline{C}_D$	$\overline{S}_t$
Blevins (1984)	–	1.20	0.19
Mustto et al. (1998)	–	1.22	0.22
Alcântara Pereira et al. (2002)	0.04	1.21	0.22
Present simulation	0.06	1.20	0.19

Source: The authors.

The numerical results represent average values calculated from t = 10 to t = 40 of the numerical simulation. As can be observed all the numerical obtained results are consistent with the ones obtained experimentally. The drag coefficient is about 1.2, while the lift coefficient is almost zero, as it should be.

The Strouhal number, which measures the frequency of vortex shedding f, is defined as usual and, for future use a body Strouhal number is also defined

$$S_t = \frac{Uf}{d} \quad S_{tc} = \frac{Uf_c}{d} \quad 2\pi f_c = \omega \tag{23}$$

Figure 2 shows the pressure distribution on the cylinder surface. As can be noted the obtained values follows closely the ones obtained experimentally; there are some small discrepancies from 60° to 80° which probably could be reduced with a proper turbulence modeling.
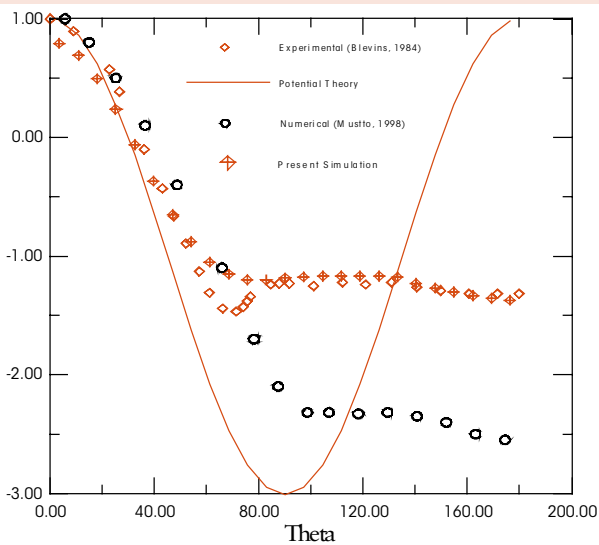
Figure 2: Comparison of the circular cylinder case, experimental and numerical results of C_p, for Re=10^5

Source: The authors.

Table 2 shows samples of results obtained. CASE I are the results for a stand still cylinder, CASE II represents typical values for small amplitude (A=0.15) motions while CASE III refers to a large amplitude (A=0.5) motions.

A significant range of the cylinder oscillation frequency is covered in this table. A careful analysis of the Strouhal number (S_t) shows three different flow regimes. For low frequency of the body oscillation (low value of S_{tc}) the S_t value is very close to 0.19, the stand still value for the Strouhal number. On the other extreme, for high value o S_{tc}, lock-in is observed and the vortex shedding frequency is equal to the body oscillation frequency. Between these two extreme there is a transition regime with no definite behavior could be observed; lock-in could be partially observed. This is particularly clear for large amplitude motions as illustrated in Figure 3.

Table 2: Circular cylinder: results for an oscillatory motion, Re = 10^5

CASE	Amplitude (A)	Angular Velocity (ω)	$\overline{C_L}$	$\overline{C_D}$	$\overline{S_{tc}}$	$\overline{S_t}$
I	0	0	0.06	1.20	0	0.19
II	0.15	0.02	0.0928	1.2572	0.00318	0.1912
		0.05	0.0846	1.2054	0.00796	0.1901
		0.1	0.0706	1.2270	0.01592	0.2128
		0.2	-0.0430	1.2430	0.03183	0.2016
		0.3	-0.0291	1.2049	0.04775	0.1961
		0.4	0.0049	1.1622	0.06366	0.1947
		0.6	-0.0256	1.0553	0.09549	0.1988
		0.9	-0.0272	1.0080	0.14324	0.1399
		1.2	0.0102	1.2988	0.19099	0.1908
		1.5	0.0062	1.0211	0.23873	0.2395
III	0.5	0.02	0.0286	1.2360	0.00318	0,1968
		0.05	0.1024	1.1635	0.00796	0,1950
		0.1	0.0931	1.1953	0.01592	0,1980
		0.2	0.0040	1.0997	0.03183	0,2051
		0.4	0.0034	0.5936	0.06366	0,0766
		0.6	0.1809	0.4512	0.09549	0,0948
		0.9	0.0785	0.9328	0.14324	0,1435
		1.2	0.0095	0.8443	0.19099	0,1876
		1.5	0.1380	0.5499	0.23873	0,2410

Source: The authors.
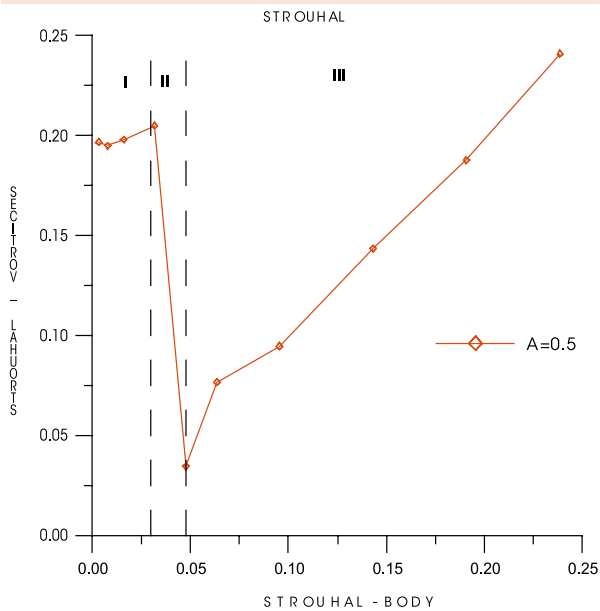
Figure 3: Strouhal number behavior as a function of the body oscillation frequency, Re = 10^5
Source: The authors.

To better understand what is happening, let us start analyzing the flow behind a stand still cylinder. From each side of the symmetry line (x-axis passing through the cylinder center) large structures formed by clusters of point vortices are shed alternately forming the Karmann vortex street. For low frequency of the body oscillation, the behavior is almost the same although the positions of the cluster shedding move according to the oscillation amplitude; this is shown in Figure 4.

Figure 4: Wake pattern when the body oscillates with small amplitude and low frequency, Re = 10^5
Source: The authors.

For a heaving cylinder in the transition regime, the wake structure becomes intermittent

and the vortex clusters are shed irregularly from the cylinder.

For the lock-in regime a high strength cluster of vortices just behind the cylinder is observed when it passes through the symmetry line; this situation is illustrated in Figure 7, when the cylinder is moving from top to bottom. This cluster – referred as the actual cluster – has a slow rotation in the anti-clockwise direction which decelerates the flow in the upper part of the cylinder and accelerates the flow in the lower part; thus vorticity is fed into a new cluster, which has started to develop in the upper part, enhancing its strength. This newly developed cluster pushes the actual cluster and when the cylinder reaches its lower position it separates into the wake, see Figure 5. This figure shows the near field wake pattern at t = 15, when the cylinder is its lowest position.

Of course, the opposite is observed when the cylinder is moving from its lower position to the upper position; Figure 6 shows the near field wake pattern at t = 23, when the cylinder is in its uppermost position.

Figure 8 is assembled with the data from the same simulation used in the previous figure; it is presented to illustrate the lift coefficient behavior during the numerical simulation. As can be observed, the lift coefficient oscillates with the same frequency of the body oscillation and its amplitude can reach values as high as 1.5 to 2.0. In this figure, the black line is the cylinder motion and the blue one is the lift coefficient.

Figure 5: Cylinder in its lowest position (t = 15, when ω = 1.5 and A = 0.5)
Source: The authors.
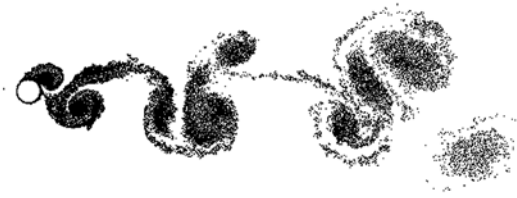
Figure 6: Cylinder in its uppermost position (t = 25, when ω = 1.5 and A = 0.5)
Source: The authors.

Figure 7: Center of the cylinder passing through the symmetry line in the downward motion (t = 30, when ω = 1.5 and A = 0.5)
Source: The authors.

Figure 8: Lift coefficient during the numerical simulation
Source: The authors.

The data from Table 2 also shows a reducing trend in the drag coefficient as the frequency of the cylinder oscillation increase. No solid explanation can be presented about this subject at this moment.

6 Conclusions

The three-dimensional effects present in the experiments are very important for the Reynolds number used in the simulations. Therefore a purely two-dimensional computation of the flow must produce differences in the comparison of the numerical results with the experimental results. The differences encountered in the comparison of the computed values with the experimental results for the distribution of the mean pressure coefficient along the cylinder surface as shown in Figure 2 are attributed mainly to the inherent three-dimensionality of the real flow for such a value of the Reynolds number, which is not modeled in the simulation.

The results for the pressure distribution indicated that there was a lack of resolution near the stagnation point and the position of the separation point. The position of the separation point is predicted to occur at about 78°, whereas the experimental value (Blevins, 1984) is about 82°. This seems to indicate that a higher value of M would improve the resolution and probably produce a better simulation with respect to the pressure distribution. More investigations are needed and one can imagine that with the use of more panels (and therefore more free vortices in the cloud) the results tend to be in closer agreement with the experiments.

Some discrepancies observed in the determination of the aerodynamics loads may be also attributed to errors in the treatment of vortex element moving away from a solid surface. Because every vortex element has different strength of vorticity, it will diffuse to different location in the flow field. It seems impossible that every vortex element will move to same ε-layer normal to the

solid surface. In the present method all nascent vortices were placed into the cloud through a displacement $\varepsilon = \sigma_0 = 0.0009b$ normal to the panels.

The use of a fast summation scheme to determine the vortex-induced velocity, such as the Multiple Expansion scheme, allows an increase in the number of vortices and a reduction of the time step, which increases the resolution of the simulation, in addition to a reduction of the CPU time, which allows a longer simulation time to be carried out. The present calculation required 9 h of CPU time in an Intel(R) Pentium(R) 4 CPU 1700 MHz.

The sub-grid turbulence modeling is of significant importance for the numerical simulation. The results of this analysis, taking into account the sub-grid turbulence modeling, are also being generated and will be presented in due time, elsewhere.

Finally, despite the differences presented in this preliminary investigation, the results are promising, that encourages performing additional tests in order to explore the phenomena in more details.

7 Acknowledgement

References

ALCÂNTARA PEREIRA, L. A.; RICCI, J. E. R.; HIRATA, M. H.; SILVEIRA-NETO, A. Simulation of Vortex-Shedding Flow about a Circular Cylinder with Turbulence Modeling, *Intern'l Society of CFD*, v. 11, n. 3, p. 315-322, Oct. 2002.

BLEVINS, R. D. *Applied fluid dynamics hanbook*. Van Nostrand Reinhold Co., 1984,

CHORIN, A. J. Numerical Study of Slightly Viscous Flow, *Journal of Fluid Mechanics*, v. 57, p. 785-796, 1973.

FERZIGER, J. H. *Numerical Methods for Engineering Application*, John Wiley & Sons, 1981.

HIRATA, M. H.; OLIVEIRA, W.; RICCI, J. E. R.; ALCÂNTARA PEREIRA, L. A. *Método de vórtices*, CD do Departamento de Mecânica, IEM, Unifei, Itajubá, MG, Brasil, 2003.

KAMEMOTO, K. *On Contribution of Advanced Vortex Element Methods Toward Virtual Reality of Unsteady Vortical Flows in the New Generation of CFD*, Proceedings of the 10th Brazilian Congress of Thermal Sciences and Engineering-ENCIT 2004, Rio de Janeiro, Brazil, Nov. 29 – Dec. 03, 2004, Invited Lecture-CIT04-IL04.

KAMEMOTO, K. *Development of vortex methods for grid-free lagrangian direct numerical simulation,* Proceedings of the 3th. JSME-KSME Fluids Engeneering Conference, Sendai, Japan, July 25-27 1994.

LEWIS, R. I. *Vortex Element Methods, the Most Natural Approach to Flow Simulation – A Review of Methodology with Applications*, Proceedings of 1st Int. Conference on Vortex Methods, Kobe, Nov. 4-5 1999, p. 1-15.

LEWIS, R. I. *Vortex Element Method for Fluid Dynamic Analysis of Engineering Systems*. Cambridge, England, U.K: Cambridge Univ. Press, 1991.

MUSTTO, A. A.; HIRATA, M. H.; BODSTEIN, G. C. R. *Discrete Vortex Method Simulation of the Flow Around a Circular Cylinder with and without Rotation*, A.I.A.A. Paper 98-2409, Proceedings of the 16th A.I.A.A. Applied Aerodynamics Conference, Albuquerque, NM, USA, June 1998.

RICCI, J. E. R. *Numerical Simulation of the Flow Around a Body in the Vicinity of a Plane Using Vortex Method*, PhD Thesis, Mechanical Engineering Institute, Universidade Federal de Itajubá, Itajubá, MG, Brazil, 2002. (in Portuguese).

SARPKAYA, T. Vortex Element Method for Flow simulation, *Advances in applied Mechanics*, v. 31, p. 113-247, 1994.

SHINTANI, M.; AKAMATSU, T. Investigation of two dimensional discrete vortex method with viscous diffusion model, Computational Fluid Dynamics Journal, v. 3, n. 2, p. 237-254, 1994.

SILVA, H. *Análise do escoamento ao redor de um corpo oscilante que se desloca com velocidade constante*. In: M.Sc.Dissertation, Universidade Federal de Itajubá, Itajubá, MG, Brasil, 2004.

UHLMAN, J. S. *An Integral Equation Formulation of the Equation of an Incompressible Fluid,* Naval Undersea Warfare Center, 1992, T.R. 10-086.

WILLIAMSON, C. H. K.; ROSHKO, A. Vortex formation in the wake of an oscillating cylinder, *J. Fluids and Structures*, v. 2, p. 239-381, 1988.